Article

Dip Phenomenon in High-Curved Turbulent Flows and Application of Entropy Theory

Donatella Termini [1,*] **and Tommaso Moramarco** [2] (iD)

[1] Dipartimento di Ingegneria Civile, Ambientale e Aerospaziale, University of Palermo, Viale delle Scienze, 90128 Palermo, Italy

[2] Research Institute for Geo-Hydrological Protection, CNR, Via Madonna Alta, 126, 06128 Perugia, Italy; Tommaso.Moramarco@irpi.cnr.it

* Correspondence: donatella.termini@unipa.it; Tel.: +39-328-727-4471

Abstract: The estimation of velocity profile in turbulent open channels is a difficult task due to the significant effects of the secondary flow. The present paper investigates the mechanism of the velocity-dip phenomenon, whereby the location of the maximum velocity appears to be below the free surface. Previous studies conducted in straight channels relate the mechanism of the velocity-dip phenomenon to secondary flow induced by anisotropy of turbulence. This work focuses on high-curved channels where the secondary motion, which is also induced by the channel's curvature, evolves along the bend. The width-to-depth ratio, B/h, is one of the most important parameters that are affecting the secondary motion entity. In particular, the present study aims to investigate the evolution of the velocity-dip along the bend for two values of the width-to-depth ratio and the applicability of the entropic model for the dip-phenomenon estimation. The results show that the velocity-dip is more accentuated for low values of the width-to-depth ratio, where the secondary motion plays a fundamental role in the distribution of the downstream flow velocity, although the velocity-dip is also present when the aspect ratio is higher than 10. Furthermore, the velocity profiles that were estimated by applying the entropic model are in good agreement with the measured ones, especially for $B/h < 10$.

Keywords: rivers; meanders; turbulence; secondary motion; prediction

1. Introduction

The understanding of flow characteristics in different bed and plane shape conditions is very important in hydraulic engineering practice. In fact, the identification of such characteristics is useful in understanding the nature of turbulence and consequent transport processes.

Literature shows (among others [1,2]) that the turbulent structure in open-channel flows can be divided into three sub-regions: a wall region, which is controlled by the inner variables (flow viscosity, local shear velocity, distance normal to the boundary); an intermediate region, which is controlled both by wall and free surface proprieties; a free surface region, which is controlled by outer variables (flow depth, maximum or mean velocity).

The log law is universally accepted for the velocity distribution in the inner region; experiments (see in [2]) show that in the outer region the velocity data deviate from the log law. To express the velocity distribution in both the inner and outer regions, some authors ([3–7]) suggested including an additional term, called the wake term.

Some researchers ([8,9]), analyzing the velocity field and the importance of secondary currents over three-dimensional bedforms, also highlighted a deviation of flow from the logarithm behavior.

The effect of the free surface on turbulence is particularly important ([10,11]). Literature widely reports on the velocity-dip phenomenon due to the position of the maximum velocity below the

water surface (among others [12,13]). Although experiments (among others [13]) demonstrate that the velocity-dip phenomenon occurs if the aspect ratio of the channel width to the water depth, B/h, is less than 5 (see as an example in [14]), some authors (among others [15,16]) have highlighted that it occurs near the side-walls, even if B/h is large. Generally, the velocity-dip increases passing from the channel axis to the side-walls. Yan et al. [17] experimentally investigated the influence of the distance from the sidewalls on the dip-position, for different values of the aspect ratios. Their results substantially validated the classification of wide and narrow open-channel flows [13], identifying two different regions in the flow field: the strong sidewall region, where the dip-position is affected only by the distance from the sidewalls; the weak sidewall region, where the dip-position is affected both by the distance from the sidewalls and by the aspect ratio.

Thus, in summary, different factors (such as the walls roughness, the distance from the sidewalls, the aspect ratio, the free-surface effect) could affect the formation and position of the velocity-dip.

The log law cannot account for the velocity-dip phenomenon and different formulations to describe the vertical distribution of longitudinal velocities in the narrow channels (i.e., for low width-to-depth ratios) can be found in literature. As an example, Yang et al. [16] proposed a dip-modified log law depending on a dip correction factor; Bonakdari et al. [18] and Absi [19] presented new formulations for the velocity distribution and dip phenomenon based on the Navier–Stokes equations. Kundu [20] presented an analytical model to predict the dip-position through the maximization of the entropy function and assuming the dip as a random variable. As discussed in [20], Kundu's model allows for the estimation of the dip-position with an accuracy that is similar to that obtained by using Yang et al.' [16] formulation.

However, the suggested models require different parameters that limit their application. Furthermore, the major part of studies that were conducted to investigate the dip phenomenon considered uniform flows in straight channels; the dip phenomenon was often related to the secondary currents, which transport low momentum fluids from the near bank region to the center and high momentum fluids from the free surface to the bed ([2,21,22]). Recently, Yang and Lee [23], analyzing the kinematic behavior of non-uniform (accelerating/decelerating) straight flows, suggested to describe the velocity-dip phenomenon through the Reynolds shear stress distribution. More recently, Moramarco et al. [24] presented a new methodology to estimate the velocity profile and the velocity-dip starting from the surface velocity evaluation. Such a methodology was based on the entropic theory, and thus, on the linear relationship between the maximum velocity, u_{max}, and the mean flow velocity, u_m, through a dimensionless function $\Phi(M)$, depending on the entropic parameter, M ([25–29]).

The point is that the mechanism of dip phenomenon is not well known still today. More research on the velocity-dip mechanism and its relation with secondary motion is needed.

In such a context, the objective of the present work is to gain some insight into the relation between the velocity-dip and secondary motion in accelerating/decelerating flows. In particular, this paper focuses on high-curvature channels, where the variation of the turbulent activity of flow is strongly correlated with the evolution of the secondary motion, which also plays a fundamental role in the distribution of the downstream flow velocity ([30–32]). The study is motivated by the fact that meandering bends have radii of curvature continuously variable in stream-wise direction so that convective flow accelerations occur and the entity of secondary motion changes from cross-section to cross-section (see as an example in [32]). As literature shows ([33,34]), the width-to-depth ratio is one of the most important parameters affecting the entity of the secondary motion in a meandering stream. As an example, the experiments that were conducted by Hooke ([35]) highlighted that the "helix strength" increases as the ratio B/h decreases; in a large amplitude sine-generated channel, Whiting and Dietrich ([36]) found that the effect of flow convective accelerations is more important than that of secondary circulation in "wide" meandering streams, which are characterized by $B/h > 10$ ([13,34,37]). Termini ([33]), analysing the flow pattern for two values of the width-to-depth ratio in a large amplitude sine-generated laboratory flume, confirmed the aforementioned behavior.

This behavior may influence the shape of the velocity profiles, and thus the entity of the velocity-dip phenomenon, along the bend.

Thus, the specific purpose of this paper is twofold: (1) to analyze the velocity-dip phenomenon along the bend for two values of the width-to-depth ratio; and, (2) to explore the applicability of the entropic model ([24]) to estimate the velocity profile and the velocity-dip phenomenon, starting from the acknowledgment of the surface velocity.

2. Materials and Methods

2.1. Experimental Dataset

The data used in the present work were collected in the ambit of previous studies that aimed to analyze the kinematic characteristics of flow along a high-amplitude meandering channel. Details of the experimental setup and measurements conditions can be found in previous works (see as an example in [33]) and only features of particular interest for the following analyses are briefly presented here.

The channel follows the sine-generated curve with a deflection angle at the inflection section $\theta_0 = 110°$ (see Figure 1).
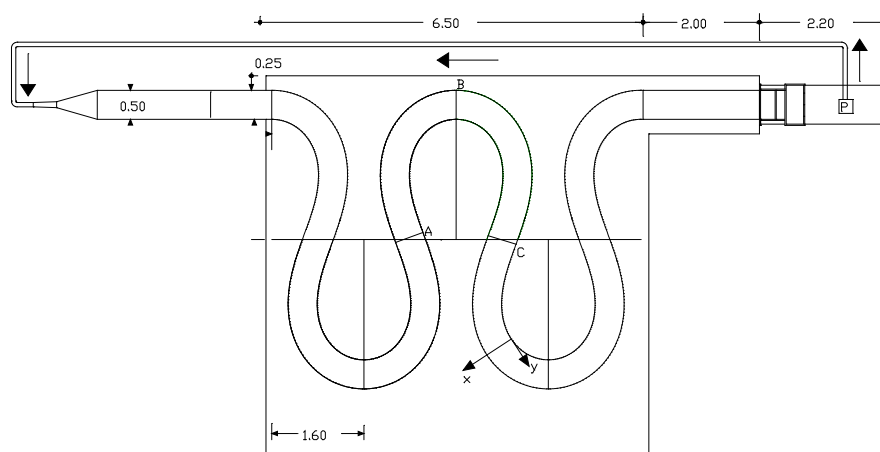

Figure 1. Experimental apparatus.

The channel cross-section is rectangular with width $B = 0.50$ m; the fixed vertical sidewalls are of plexiglass and the bed, with longitudinal centerline slope $S = 0.371\%$, is flat and made of quartz sand (d_{50} = medium sediment diameter = 0.65 mm, σ_g = geometric standard deviation = 1.34). The meandering channel is around 25 m long in order to accommodate two meander wavelengths; the upstream and downstream ends of the meandering channel are connected to two straight channels 3 m and 2 m long, respectively.

In the present paper, the data collected during two runs conducted with two different values of flow discharge have been used: Run 1 was conducted with a flow discharge of $Q = 0.019$ m^3/s (channel-averaged flow depth $h = 5.5$ cm; $B/h = 9.09 < 10$); Run 2 was conducted with a flow discharge $Q = 0.007$ m^3/s (channel-averaged flow depth $h = 3.0$ cm, $B/h = 16.67 > 10$). Herein, in accordance with other authors ([13,34]), $B/h < 10$ indicates "small" width-to-depth ratio and $B/h > 10$ indicates "large" width-to-depth ratio.

During each run, the water surface was measured using a Profiler Indicator PV09 (Delft Hydraulics) with precision of 0.1 mm. The instantaneous local longitudinal and transverse velocity components were measured in cross-sections spaced about 50 cm or so apart, starting from the first inflection section of the meandering channel (see Figure 1), by using a two-dimensional (2D) side-looking Acoustic Doppler Velocimeter (ADV) manufactured by SonTek Inc. (San Diego, CA, USA), in points spaced of 1–1.5 mm along the verticals of nine transverse abscissas symmetrically to the

channel axis (see details in [33]). Bearing in mind the specific aim of the present work, our attention is focused only on the longitudinal velocity component. Furthermore, in the present work attention concerns only two consecutive inflection sections (sections A and C of Figure 1) and the apex section B of Figure 1.

2.2. Pertinent Aspects and Summary of Previous Results

Before proceeding further, it seems important to briefly summarize here some peculiar results of investigations performed in the same meandering flume of that considered in this work:

- Termini ([33]) conducted experiments under the hydraulic conditions that are considered in the present work in order to examine the effect of the continuously changing channel's curvature on flow pattern. She verified that, because of the changing channel curvature, the flow accelerates near the outer bank from the beginning of the bend to the inflection section downstream and decelerates near the inner bank. The flow accelerated zone is more evident for $B/h > 10$ than for $B/h < 10$. Such a different behaviour is caused by the secondary circulation that develops more significantly in the case of $B/h < 10$ than in the case of $B/h > 10$, and that attenuates the effect of the convective acceleration close to the outer bank (see also in [31]).

- Termini and Moramarco ([29]) investigated the effect of the downstream variation of the channel's curvature on the applicability of the linear entropic relationship between the maximum velocity, u_{max}, and the mean flow velocity, u_m, through a dimensionless parameter $\Phi(M)$. As result, they observed that the ratio u_m/u_{max}, and thus the value of the parameter $\Phi(M)$, varies along the bend. In particular, Termini and Moramarco ([29]) demonstrated that, in contrast to what observed in straight channels ([28]) where $\Phi(M)$ assumed a value that was almost constant and on average equal to 0.65, along the meandering bend the parameter $\Phi(M)$ increases passing from the inflection section to the apex section and decreases from the apex section to the inflection section downstream, assuming a value of around 0.8 close to the apex section and of around 0.6 at the inflection section. This behavior can be observed from Figure 2, where the values of the parameter $\Phi(M)$, as obtained by Termini and Moramarco ([29]), along the bend are reported.
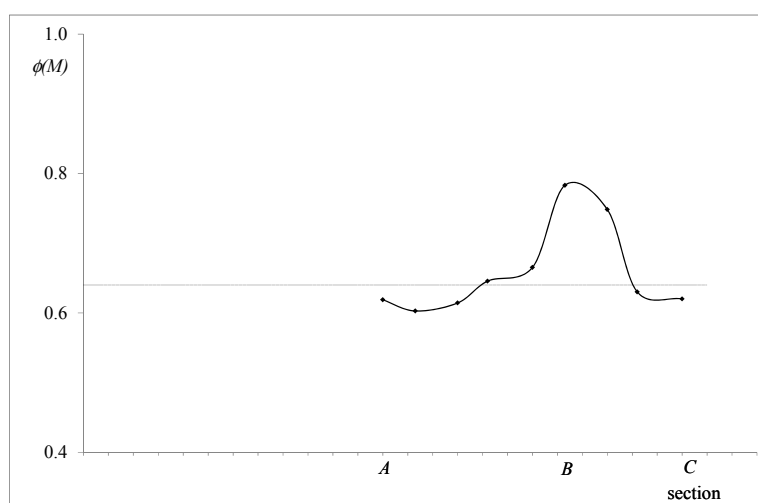

Figure 2. Values of $\Phi(M)$ obtained by Termini and Moramarco ([20]) along the meandering bend.

3. Results

3.1. Measured Velocity Profiles and Effect of the Aspect Ratio on the Velocity-Dip

The time-averaged longitudinal velocity, u, was estimated for each measurement point by using the series of the measured instantaneous longitudinal velocity component. Thus, the

u-profiles (hereafter denoted as "measured profiles") were estimated for each measurement vertical. Then, the distance δ (dip) between the maximum of flow velocity below the water surface was evaluated for each vertical measured profile.

From the analysis of all the measured profiles appeared clear that the dip-phenomenon occurs for both the width-to-depth ratios. But, the value of the dip decreases as the width-to-depth ratio increases. As an example, Figure 3 shows the velocity profiles that were measured in peculiar verticals (i.e., where the dip was evident) of the examined sections for both the aspect ratios. Furthermore, it was observed that, while in Run 1 (i.e., for $B/h < 10$) the velocity-dip is evident in all the measured profiles, in Run 2 (i.e., for $B/h > 10$), the velocity-dip is especially evident in the regions that are close to the banks. This behavior is consistent with previous literature findings obtained in straight channels (among others [2,13]).

The entity of the distance δ (dip) varies along the bend. This behavior can be observed from Table 1, where the values of the distance δ determined for each measured profile as percentage of the local flow depth are reported for both runs, and from Figure 4, which compares the δ-values that were estimated in the apex section and in the inflection sections for both the width-to-depth ratios. From Table 1 and Figure 4, it can be noted that the velocity-dip is more evident when the aspect ratio B/h is less than 10, but it is also present when the aspect ratio B/h is higher than 10. In particular, as Table 1 shows, in average, the dip assumes a value of around 53% of the flow depth in Run 1 (i.e., for $B/h < 10$) and of around 34% of the flow depth in Run 2 (i.e., for $B/h > 10$).
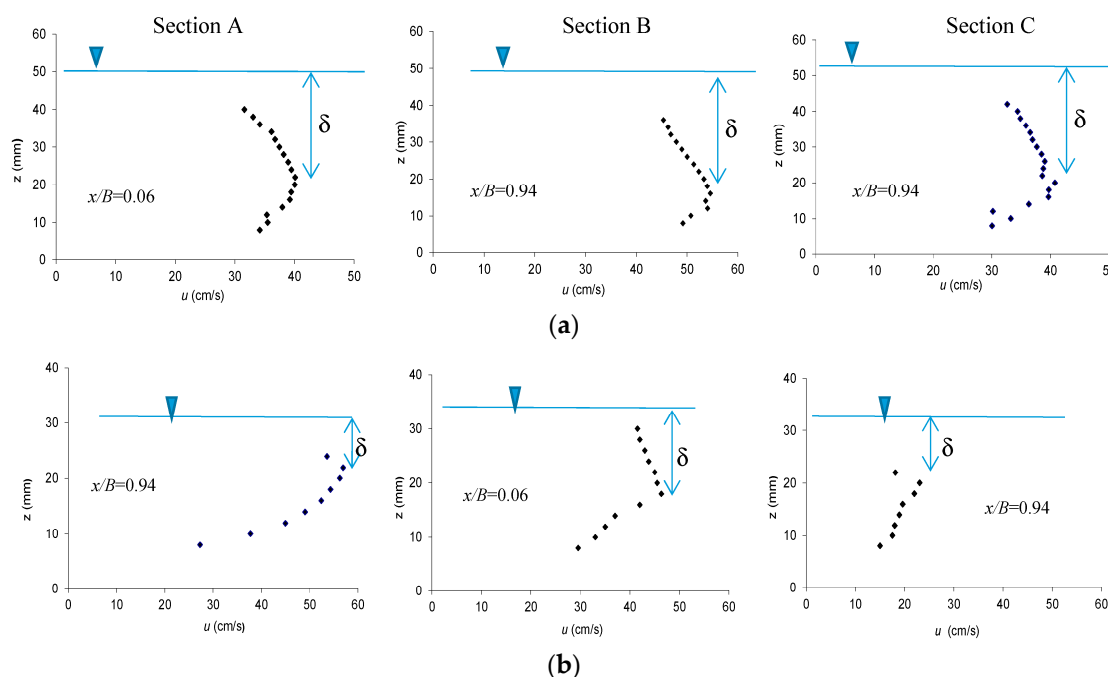

Figure 3. Measured profiles at peculiar verticals of the examined sections: (**a**) Run 1 ($B/h < 10$); (**b**) Run 2 ($B/h > 10$); x/B indicates the relative distances from the left (outer) bank.

This is probably due to the fact that, as literature demonstrates ([32,35]), the entity of the secondary circulation increases as the ratio B/h decreases. Thus, the observed behavior also indicates that the evolution of the velocity-dip phenomenon along the bend is strongly related to the evolution of the cross-sectional secondary motion along the bend itself.

Figure 4 also indicates that, for $B/h < 10$, the velocity-dip always assumes significant values: at the inflection section upstream, the velocity-dip has the higher values that are close to the left (outer) bank; at the apex section high values of the velocity-dip occur almost in the whole cross section until that at the inflection section downstream δ assumes the higher values close to the right (inner)

bank. For $B/h > 10$, the velocity-dip assumes always very small values and the higher values of the velocity-dip can be found close to the left (outer) bank at the apex section.

Table 1. δ-values estimated for each measured profile as percentage of the local flow depth.

|	δ**av (%) = 53**								
B/h < 10				*x/B*					
Section	**0.06**	**0.17**	**0.28**	**0.39**	**0.5**	**0.61**	**0.72**	**0.83**	**0.94**
A	57.36	61.24	52.94	52.85	52.94	53.40	53.85	47.47	56.52
B	53.33	43.56	35.94	43.40	44.55	58.19	52.48	60.35	64.99
C	39.62	47.26	51.81	52.94	57.20	57.69	61.83	61.17	60.78
	δ**av (%) = 34**								
B/h > 10				*x/B*					
Section	**0.06**	**0.17**	**0.28**	**0.39**	**0.5**	**0.61**	**0.72**	**0.83**	**0.94**
A	43.22	48.39	0.00	47.37	35.90	35.90	0.00	38.27	36.60
B	50.00	35.86	20.97	37.69	35.48	26.42	37.50	36.62	44.44
C	32.89	32.20	24.91	40.48	33.55	34.21	34.64	33.77	32.89

(a)

(b)
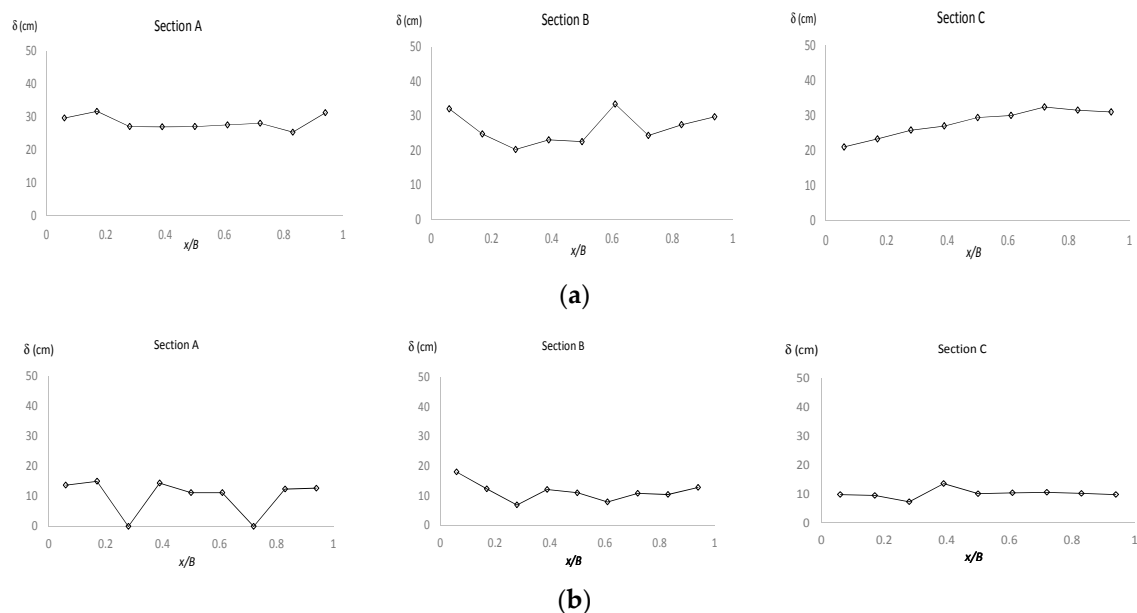
Figure 4. Velocity-dip phenomenon in each examined section: (**a**) $B/h < 10$; (**b**) $B/h > 10$.

3.2. Application of the Entropic Model to Estimate the Velocity-Dip Phenomenon

Recently, Moramarco et al. ([24]) developed an iterative procedure to estimate the velocity profile and the velocity-dip based on the entropy profile, which can be written as:

$$u(x,z) = \frac{u_{\max,v}}{M}\ln\left[1 + \left(e^M - 1\right)\frac{z}{D-\delta}\exp\left(1 - \frac{z}{D-\delta}\right)\right] \tag{1}$$

with

$$u_{\max,v} = \frac{u_{surf}}{\frac{1}{M}\ln\left[1 + (e^M - 1)\delta e^{1-\delta}\right]} \tag{2}$$

where $u_{max,v}$ is the maximum velocity along the each measurement vertical, D is the water depth, z is the distance of the velocity point from the bed, x is the distance of the considered vertical from the left bank, and M is the entropic parameter, which can be estimated by using the entropic relation ([25]):

$$u_m = \left(\frac{e^M}{e^M - 1} - \frac{1}{M} \right) u_{\max} = \phi(M) u_{max} \qquad (3)$$

where $u_{max} = \max[u_{max,v}]$ which is located at z-axis. The velocity-dip is estimated by using the modified expression proposed by Yang et al. ([16]), written as ([24]):

$$\delta'(x) = a_p + \delta(x) \text{ with } \delta = 1 + 1.3 e^{-x/D} \qquad (4)$$

where a_p is an iterative parameter representing the dip at z-axis, and which is updated at each iteration, p, by adding a constant value (0.001 m), and starting from the initial value $a_1 = 0.0001$.

By inspecting Equations (1)–(4), it is clear that, in contrast to other formulations that are proposed in literature to estimate the velocity profile and the velocity-dip (among others [4,12,13]), the aforementioned procedure only depends on parameters that have a clear physical meaning and are easily measurable.

Starting from the observed surface velocity, u_{surf}, and the knowledge of $\Phi(M)$, the maximum velocity $u_{max,v}$ and the velocity-dip are computed, respectively, through Equations (2) and (4) by initializing $a_p = a_1$. Then, the velocity profiles are computed through Equation (1) and the maximum velocity $u_{max} = \max[u_{max,v}]$ is assessed. Once the velocity profiles are identified, the mean flow velocity, u_m, can be assessed by applying the velocity area method ([38]) at the estimated velocity profiles; therefore, the ratio $\Phi_{com}(M_1) = \frac{u_m(a_1)}{u_{max}(a_1)}$ can be computed by Equation (3). The iterative procedure ends when the optimal value of $\Phi_{com}(M_p)$ is achieved in accordance with:

$$\Phi(M_{obs}) - \Phi(M_p) = \text{minimum} \qquad (5)$$

Thus, for each measurement vertical and for each run, the velocity profiles (hereon called as "estimated velocity profiles") have been determined by applying the aforementioned iteration procedure and starting from the acknowledgment of the measured surface velocity. Figure 5 shows, as an example, the comparison between the measured and the estimated velocity profiles in the selected measurement verticals. From this figure, it can be observed that the estimated velocity profiles are in good agreement with the measured ones. This is especially evident in the case of $B/h < 10$.
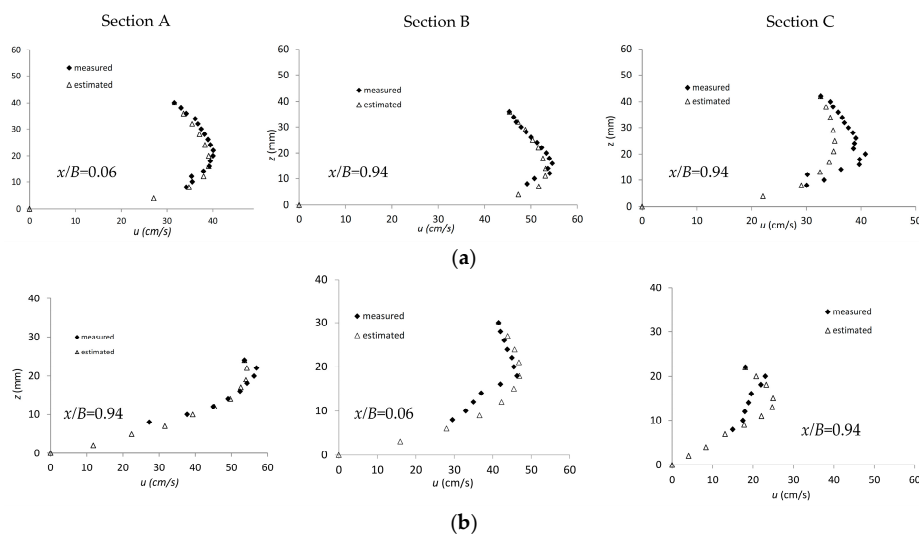

Figure 5. Comparison between measured and estimated profiles: (**a**) $B/h < 10$; (**b**) $B/h > 10$.

The good fit between all of the δ-values determined from the estimated velocity profiles and those that were obtained from the measured velocity profiles has been verified by using the root mean squared error (σ) as indicator. It is:

$$\sigma = \sqrt{\frac{\sum_{i=1,N}(\delta_{i,m} - \delta_{i,e})^2}{N}} \tag{6}$$

where $\delta_{i,m}$ and $\delta_{i,e}$ are the δ-values determined, respectively, from the measured and from the estimated profiles, N is the total number of measurements that are considered for each profile. Figure 6 reports the pair of values ($\delta_{i,m}$, $\delta_{i,e}$) and the line of perfect agreement (bisector line). The error bar is defined by the value of σ. As shown in Figure 6, with a few exceptions, the points arrange around the bisector line and the σ is quite low in comparison to the magnitude of the measured values.
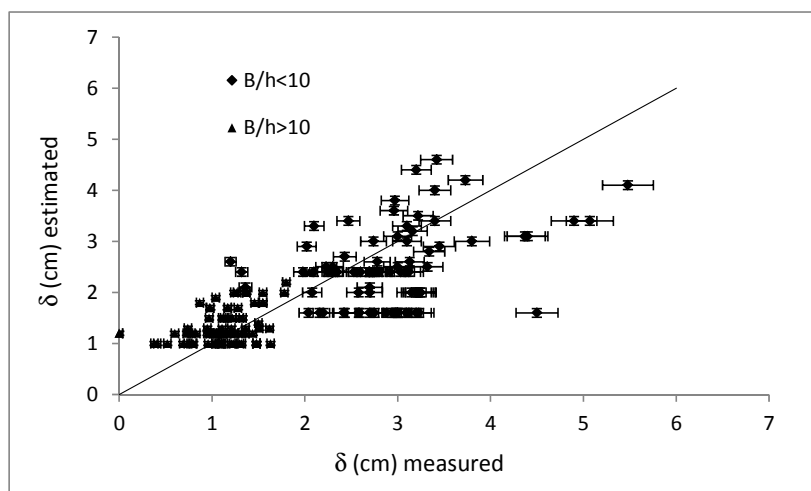

Figure 6. Comparison between estimated and measured δ-values.

4. Discussion and Concluding Remarks

The mechanism of the dip phenomenon is investigated in a high-amplitude meandering channel, which is characterized by radii of curvature continuously variable in stream-wise direction, and, as previous findings indicate (see as an example [31,32]), convective flow accelerations occur and the entity of secondary motion changes along the bend modifying the turbulent activity at the channel's boundaries.

As it should be clear from the "Introduction", previous researches that were conducted in straight channels relate the velocity-dip to the secondary currents occurring especially in narrow channels where the side-walls effect is strong. Experiments (see among others in [2,13]) show that in narrow channels the side-walls produce anisotropy of turbulence but the velocity-dip is also determined by the free-surface effect. In wide channels, there is a central area where the side-wall effect disappears and only the free-surface effect occurs.

The results obtained in this work have shown that the velocity-dip phenomenon is more accentuated for low aspect ratio ($B/h < 10$), but it is also present for large aspect ratio ($B/h > 10$). In particular, in the first case, the velocity-dip, δ, assumes always significant values, but it varies along the bend. In particular, at the inflection section upstream it is more accentuated close to the left (outer) bank; then at the apex section high values of the velocity-dip occur almost in the whole cross section until that at the inflection section downstream δ assumes the higher values close to the right (inner) bank. For high aspect ratio, the velocity-dip assumes always very small values and, in accordance with results obtained in straight channels, the dip-phenomenon assumes the lower values especially in the

central region of the cross section. Furthermore, the variation of the δ-values along the bend that were observed for high aspect ratio is less evident than that observed for low aspect ratio.

Termini ([32]), by using data collected in the same channel as that considering in the present work for $B/h < 10$, verified that, as the curvature increases along the bend, the advective momentum transport by the cross-circulation increases determining the deformation of the vertical distribution of the downstream flow velocity (see also in [30]). This behavior suggests that the evolution of the velocity-dip phenomenon along the bend is strongly related to the evolution of the cross-sectional secondary motion.

The results have also shown that the entropic model allows for adequately estimating the velocity-dip, especially in the case of $B/h < 10$. This allows for us to evaluate the velocity profile and the dip phenomenon, starting from the acknowledgment of the measured surface velocity and by considering the easily measurable parameters.

In conclusion, the reported results confirm that the velocity-dip varies along the channel depending on the variation of the secondary motion; the velocity-dip could be easily estimated through the application of the entropy model.

Based on the obtained results, future research will be oriented towards estimating the relation between the secondary motion and the entropy-evaluated velocity-dip.

References

1. Song, T.; Graf, W.H. Velocity and turbulence distribution in unsteady open-channel flows. *J. Hydraul. Eng.* **1996**, *122*, 141–154. [CrossRef]
2. Nezu, I.; Nakagawa, H. *Turbulence in Open-Channel Flows*; Balkema, A.A., Ed.; CRC Press: Rotterdam, The Netherlands, 1993.
3. Coles, D. The low of the wake in the turbulent boundary layer. *J. Fluid Mech.* **1956**, *1*, 191–226. [CrossRef]
4. Finley, P.J.; Phoe, K.C.; Poh, C.J. Velocity measurements in a thin turbulent water layer. *La Houille Blanche* **1966**, *6*, 713–721. [CrossRef]
5. Kironoto, B.A.; Graf, W.H. *Turbulence Characteristic in Rough Uniform Open-Channel Flow*; Laboratoire de Researches Hydrauliques, Ecole Polytechnique Federale: Lausanne, Switzerland, 1994.
6. Guo, J.; Julien, P.Y. Application of the modified log-wake law in open-channels. *J. Appl. Fluid Mech.* **2008**, *1*, 17–23.
7. Cioffi, F.; Gallerano, F. Velocity and concentration profiles in a channel with movable end erodible bed. *J. Hydraul. Res.* **1991**, *29*, 387–401. [CrossRef]
8. Da Silva, M.F.; Kanani, A. A study of large-scale horizontal; in alluvial streams with a view towards its morphological consequences. In *Free Surface Flows and Transport Processes, GeoPlanet: Earth and Planetary Sciences*; Springer: Berlin, Germany, 2018; pp. 1–25.
9. Najafabadi, E.F.; Afzalimehr, H.; Rowinski, P.M. Flow structure through a fluvial pool-riffle sequence—Case study. *J. Hydro-Environ. Res.* **2018**, *19*, 1–15. [CrossRef]
10. Flores, O.; Riley, J.J.; Horner-Devine, A.R. On the dynamics of turbulence near a free surface. *J. Fluid Mech.* **2017**, *821*, 248–265. [CrossRef]
11. Troiani, G.; Cioffi, F.; Casciola, C. Free surface-vorticity interactions in an open channel flow. *J. Hydraul. Eng.* **2004**, *130*, 313–323. [CrossRef]
12. Steffler, P.M.; Rajaratnam, N.; Peterson, A.W. LDA measurements in open channel flow. *J. Hydraul. Eng. ASCE* **1985**, *111*, 119–130. [CrossRef]
13. Nezu, I.; Rodi, W. Open channel flow measurements with a laser Doppler anemometer. *J. Hydraul. Eng. ASCE* **1986**, *112*, 335–355. [CrossRef]

14. Greco, M.; Moramarco, T. Influence of bed roughness and cross section geometry on medium and maximum velocity ratio in open-channel flow. *J. Hydraul. Eng. ASCE* **2016**, *142*, 06015015. [CrossRef]

15. Sarma, K.V.N.; Lakshminarayana, P.; Lakshmana Rao, N.S. Velocity distribution in smooth rectangular open channel. *J. Hydraul. Eng. ASCE* **1983**, *109*, 270–289. [CrossRef]

16. Yang, S.Q.; Tan, S.K.; Lim, S.Y. Velocity distribution and dip phenomenon in smooth uniform open channel flow. *J. Hydraul. Eng. ASCE* **2004**, *130*, 1179–1186. [CrossRef]

17. Yan, J.; Tang, H.; Xiao, Y.; Li, K.; Tian, Z. Experimental study on influence of boundary on location of maximum velocity in open channel flows. *Water Sci. Eng.* **2011**, *4*, 185–191.

18. Bonakdari, H.; Larrarte, F.; Lassabatere, L.; Joannis, C. Turbulent velocity profile in fully-developed open channel flows. *Environ. Fluid Mech.* **2008**, *8*, 1–17. [CrossRef]

19. Absi, R. An ordinary differential equation for velocity distribution and dip-phenomenon in open channel flows. *J. Hydraul. Res.* **2011**, *49*, 82–89. [CrossRef]

20. Kundu, S. Prediction of velocity-dip-position over the entire cross section of open channel flows using entropy theory. *Environ. Earth* **2017**, *76*, 363. [CrossRef]

21. Stearns, E.P. A reason why the maximum velocity of water flowing in open channels is below the surface. *Trans. ASCE* **1983**, *7*, 331–338.

22. Cardoso, A.H.; Graf, W.H.; Gust, G. Uniform flow in a smooth open channel. *J. Hydraul. Res.* **1989**, *27*, 603–616. [CrossRef]

23. Yang, S.Q.; Lee, J.W. Reynolds shear stress distributions in a gradually varied flow. *J. Hydraul. Res.* **2007**, *45*, 462–471. [CrossRef]

24. Moramarco, T.; Barbetta, S.; Tarpanelli, A. From Surface Flow Velocity Measurements to Discharge Assessment by the Entropy Theory. *Water* **2017**, *9*, 120. [CrossRef]

25. Chiu, C.L. Application of Entropy Concept in open-channel flow study. *J. Hydraul. Eng. ASCE* **1991**, *117*, 615–628. [CrossRef]

26. Xia, R. Relation between mean and maximum velocities in a natural river. *J. Hydraul. Eng. ASCE* **1997**, *123*, 720–723. [CrossRef]

27. Moramarco, T.; Saltalippi, C.; Singh, V.P. Estimation of mean velocity in natural channel based on Chiu's velocity distribution equation. *J. Hydraul. Eng. ASCE* **2004**, *9*, 42–50. [CrossRef]

28. Moramarco, T.; Termini, D. Entropic approach to estimate the mean flow velocity:experimental investigation in laboratory flumes. *Environ. Fluid Mech.* **2015**, *15*, 1163–1179. [CrossRef]

29. Termini, D.; Moramarco, T. Application of entropic approach to estimate the mean flow velocity and Manning roughness coefficient in a high-curvature flume. *Hydrol. Res. Dec.* **2016**, *2016*. [CrossRef]

30. Blanckaert, K.; Graf, W.H. Momentum transport in sharp open-channel bends. *J. Hydraul. Eng. ASCE* **2004**, *130*, 186–198. [CrossRef]

31. Termini, D.; Piraino, M. Experimental analysis of cross-sectional flow motion in a large amplitude meandering bend. *Earth Surf. Process. Landf.* **2011**, *36*, 244–256. [CrossRef]

32. Termini, D. Momentum transport and bed shear stress distribution in a meandering bend: Experimental analysis in a laboratory flume. *Adv. Water Resour.* **2015**. [CrossRef]

33. Termini, D. Experimental observations of Flow and Bed processes in a Large-amplitude Meandering Flume. *J. Hydraul. Eng. ASCE* **2009**, *135*, 575–587. [CrossRef]

34. Yalin, M.S. *River Mechanics*; Pregamon Press: London, UK, 1992.

35. Hooke, R.L. Distribution of sediment transport and shear stress in a meander bend. *J. Geol.* **1975**, *83*, 543–565. [CrossRef]

36. Whiting, P.J.; Dietrich, W.E. Experimental Studies of Bed Topography and Flow Patterns in Large-Amplitude Meanders, 1. Observations. *Water Resour. Res.* **1993**, *29*, 3605–3614. [CrossRef]

37. Da Silva, A.M.F.; El-Tahawy, T.; Tape, W.D. Variations of flow pattern with sinuosity in sine-generated meandering streams. *J. Hydraul. Eng. ASCE* **2006**, *132*, 1003–1014. [CrossRef]

38. Herschy, R.W. *Streamflow Measurement*; Elsevier: London, UK, 1985.